Exchange bias in molecule/Fe_3GeTe_2 van der Waals heterostructures via spinterface effects

Junhyeon Jo, Francesco Calavalle, Beatriz Martín-García, Daniel Tezze, Fèlix Casanova, Andrey Chuvilin, Luis E. Hueso*, and Marco Gobbi**

Dr. J. Jo, Dr. F. Calavalle, Dr. B. Martín-García, D. Tezze, Prof. F. Casanova, Prof. A. Chuvilin, Prof. L. E. Hueso, Dr. M. Gobbi

CIC nanoGUNE, 20018 Donostia-San Sebastian, Basque Country, Spain

E-mail: j.jo@nanogune.eu; l.hueso@nanogune.eu; m.gobbi@nanogune.eu

Prof. F. Casanova, Prof. A. Chuvilin, Prof. L. E. Hueso, Dr. M. Gobbi

IKERBASQUE, Basque Foundation for Science, 48013 Bilbao, Basque Country, Spain

Dr. M. Gobbi

Centro de Física de Materiales (CFM-MPC) Centro Mixto CSIC-UPV/EHU, San Sebastián/Donostia 20018, Spain

Keywords: 2D magnets, Fe_3GeTe_2, spinterface, exchange bias, hybrid van der Waals heterostructures, Co-phthalocyanine (CoPc)

The exfoliation of layered magnetic materials generates atomically thin flakes characterized by an ultrahigh surface sensitivity, which makes their magnetic properties tunable via external stimuli, such as electrostatic gating and proximity effects. Another powerful approach to engineer magnetic materials is molecular functionalization, generating hybrid interfaces with tailored magnetic interactions, called spinterfaces. However, spinterface effects have not yet been explored on layered magnetic materials.

Here, we demonstrate the emergence of spinterface effects at the interface between flakes of the prototypical layered magnetic metal Fe_3GeTe_2 and thin films of Co-phthalocyanine. Magnetotransport measurements show that the molecular layer induces a magnetic exchange bias in Fe_3GeTe_2, indicating that the unpaired spins in Co-phthalocyanine develop antiferromagnetic ordering and pin the magnetization reversal of Fe_3GeTe_2 via magnetic proximity. The effect is strongest for a Fe_3GeTe_2 thickness of 20 nm, for which the exchange bias field reaches –840 Oe at 10 K and is measurable up to approximately 110 K. This value compares very favorably with previous exchange bias fields reported for Fe_3GeTe_2 in all-inorganic van der Waals heterostructures, demonstrating the potential of molecular functionalization to tailor the magnetism of van der Waals layered materials.

1. Introduction

The exfoliation of layered magnetic materials yields ultrathin single crystalline flakes,[1,2] which represent an ideal playground to explore magnetism in reduced dimensions.[3–6] In this materials family, Fe_3GeTe_2 (FGT) is a particularly intriguing compound, since it is a ferromagnetic metal characterized by a Curie temperature close to the room temperature and strong out-of-plane anisotropy.[7–10] Moreover, the magnetic properties of FGT are tunable, as they can be modified either electrically, applying a gate voltage[11] and a large electrical current,[12] or through magnetic proximity effects.[13–16] In particular, when interfaced with antiferromagnetic layered materials, FGT displays an increased coercivity and exchange bias, [13–16] which are the prototypical manifestation of magnetic proximity[17–19] and are key elements in spintronic devices.[20]

Another attractive approach to tune the properties of a magnetic surface is molecular functionalization.[21,22] The interfaces between magnetic materials and molecules, often named spinterfaces,[21,22] host hybrid states or magnetic interactions which lead to radical changes on the magnetic properties of both the molecular layer[23–30] and the magnetic material.[27–33] So far, the ferromagnetic layers used for investigating spinterface effects are typically films of 3*d* metals or oxides with dangling bonds on the surface, which result in non-ideal interfaces with molecules. Moreover, until recently, the molecular side of a spinterface has been the main target of research due to its easily tunable electronic properties,[23–29] whereas the possibility of tailoring the magnetism of ferromagnetic materials has yet to be fully exploited.

Layered magnetic materials are excellent candidates for developing a spinterface in view of their tunable magnetism and their single crystalline nature, which offer the possibility to form highly controllable interfaces with molecules[34,35] via the so-called van der Waals epitaxy.[36–39] Indeed, hybrid heterostructures based on atomically sharp 2D material/molecule interfaces

have been widely used to tailor the opto-electronic and transport properties of non-magnetic layered materials.[40–45] However, so far the possibility to tune the properties of a layered magnetic material through the magnetic interactions at a van der Waals spinterface has not yet been experimentally demonstrated.

Here, we report on the emergence of spinterface effects between molecular films of Co-phthalocyanine (CoPc) and a few-nm-thick FGT flakes. The molecular layer induces a negative magnetic exchange bias in FGT, indicating that the unpaired spins in CoPc develop antiferromagnetic interlayer ordering, and couple ferromagnetically to FGT via magnetic proximity. This spinterface effect, which is detected via magnetotransport measurements, is characterized by an exchange field as large as -840 Oe at 10 K, and a blocking temperature of 110 K. These characteristic values are both among the largest reported in the context of layered magnetic materials.[13–16,46–48] The creation of a molecular spinterface with a layered magnetic material opens a new avenue to tailor the magnetism of layered materials towards hybrid low-dimensional functional devices.

2. Results and Discussion

Several studies show that exchange bias emerges at the interface between ferromagnetic metals and organometallic molecules,[27–29,49] due to an antiferromagnetic ordering of molecular spins, which pin the magnetization reversal. Among the organometallic compounds used for these exploring spin-effects,[50] metallo-phthalocyanine (MPc) are a versatile class of planar semiconducting molecules widely utilized in research and industry (**Figure 1**a). The metal ion (M^{2+}) at the center of the molecule, usually a transition metal such as Co, Cu, or Zn, provides diverse energy levels, charge mobility, and spin states.[50–52] To explore the emergence of exchange bias at a FGT interface (Figure 1b), we used CoPc, which possesses a

spin $S = ½$. Importantly, in the CoPc's structural α-phase, the molecular unpaired spins develop antiferromagnetic ordering up to a relatively high temperature (~ 210 K in ref.[53] and ~ 110 K in refs.[54,55]).

For the fabrication of devices based on CoPc/FGT interfaces, we first deposited CoPc molecules on a Si/SiO_2 substrate with Au electrodes prepatterned in a Hall bar design (see Methods for details). Viscoelastic stamping with polydimethylsiloxane (PDMS) was used to mechanically exfoliate a FGT flake and transfer it onto the CoPc-covered substrate. The so-obtained CoPc/FGT structure was encapsulated with a hBN flake. The stamping processes were performed in an Ar-filled glovebox, to prevent the oxidation of FGT in air. **Figure 2**a shows the optical image of a fabricated CoPc/FGT device. The 6-nm-thick CoPc layer covered the whole area observed in this image, while the 20-nm-thick FGT and hBN layers are highlighted by a red and black line, respectively.

The integrity of the CoPc film was confirmed through microRaman spectroscopy. Figure 2b shows a comparison of the Raman spectra measured in different regions of the CoPc film, either covered by FGT/hBN (CoPc/FGT/hBN) or left uncovered (CoPc). In both regions, the spectra display the typical features of MPc molecules, indicating that the stamping process did not significantly affect the integrity of the molecular layer. In particular, the peaks of 1465 cm^{-1} and 1542 cm^{-1} represent the B_{1g} and B_{2g} mode of the CoPc molecule, and correspond to the C-N stretching directly associated to the central Co ion (detailed description in Figure S1, Supporting Information).[56]

The Raman features in the spectral range between 600 cm^{-1} and 800 cm^{-1} also provide insight on the structural arrangement of the molecular layer. In particular, the peak at 751 cm^{-1} is less intense than that at 682 cm^{-1}, indicating that the molecular film is in the structural α-phase.[57,58] This finding is confirmed by X-ray diffractometry, where a single peak at 6.7° is

observed (Figure S2, Supporting Information). This diffraction pattern is analogous to that reported by Serri et al. for CoPc molecules arranged in the α-phase with an edge-on configuration on SiO_2.[55]

Moreover, the analysis of the intensity of the Raman features provides us with another important structural information. We note that to compare the intensity of the spectra displayed in Figure 2b, we normalized them to the intensity of the Si peak at 520 cm^{-1} (see also Figure S1, Supporting Information). The molecular peaks in the CoPc layer below FGT are significantly more intense than in the uncovered region. This trend is also observed for the Raman spectra measured with a 633 nm excitation (Figure S1, Supporting Information). A similar enhancement was reported for Pc molecules lying flat on the van der Waals surface on graphene and other 2D materials.[59,60] Moreover, the enhancement is particularly pronounced for the peaks related to in-plane molecular vibrations, including the B_{1g} and B_{2g} modes at 1542 cm^{-1} and at 1465 cm^{-1}. In a previous study, the increased intensity of these modes was associated to a reorganization of Pc molecules from an edge-on to a face-on arrangement on graphene.[61] Overall, these data suggest that the stamping of FGT induces a local rearrangement of the uppermost molecular layer, which reorganizes to lie flat at the interface with FGT (Figure S2, Supporting Information).

Figure 2c displays the Raman features of a hBN-capped FGT flake transferred on a CoPc film or on a bare SiO_2 substrate. The two flakes displayed the two dominant Raman peaks of FGT at 120 cm^{-1} and 155 cm^{-1} associated to the A_{1g} and E_{2g} vibrations.[62] Even in this case, there was no significant change in the spectra for FGT in contact with CoPc or SiO_2. In addition, we mapped the intensity of the CoPc peak at 1542 cm^{-1} (Figure 2d) in the area denoted by a white dotted line in Figure 2a. The homogeneity of the intensity in the map implies that the CoPc molecules are uniformly distributed in the CoPc/hBN and CoPc/FGT/hBN regions. We note that the lower intensity of the CoPc features in the CoPc/FGT/hBN region is caused by

screening from the opaque FGT flake. These data show that the stamping process also maintains the uniformity of the molecular layer.

Scanning transmission electron microscopy (STEM) was employed to gain additional insights on the CoPc/FGT interface. Figure 2e displays a cross-sectional image of a CoPc/FGT/hBN heterostructure obtained by STEM. A low-magnification image provides a picture of the CoPc/FGT/hBN heterostructure on a Si/SiO_2 substrate, showing that the CoPc molecules constitute a compact film on SiO_2 and form a homogeneous interface with the FGT flake stamped on the top. Figure 2e also shows how the FGT flake is slightly bent to accommodate the height difference in the sample, being in contact with both the top of the pre-patterned electrodes and with the surface of the CoPc layer on SiO_2. Moreover, it is clear that the CoPc layer does not evenly cover the rough Au electrode, which in some regions is in direct contact with the FGT flake. Since both Au and FGT are good electrical conductors, even a small contact area ensures an efficient charge injection, displaying ohmic characteristics with a typical contact resistance of 1 kΩ - 2 kΩ. Enlargement of the STEM image in the right section of Figure 2e highlights the formation of a flat and uniform CoPc/FGT layer structure, which is a crucial factor to generate a spinterface effect between these layers.

To investigate the molecular spinterface effect in CoPc/FGT heterostructures, we have characterized the magnetic hysteresis of FGT flakes through magnetotransport measurement, by recording their anomalous Hall effect (AHE). We employed a specific procedure to identify the magnetic interaction at the CoPc/FGT interface. First, we performed a magnetic field-cooling (FC) process to a molecule/ferromagnetic Hall bar device from 300 K to 10 K under an out-of-plane magnetic field (H_z) of ±10 kOe, which was used to align the spins in this system. Then, we applied an electrical current (I) along a certain physical direction in the

FGT device (hereby *x*-axis) and a magnetic field in the out-of-plane direction (*z*-axis) (**Figure 3**a). By measuring the transverse Hall voltage (V_{xy}), we were able to record the Hall resistance ($R_{xy}= V_{xy}/I$) as a function of the magnetic field. In this way, we could detect the hysteresis of FGT via the AHE and relate it to the magnetic response at the CoPc/FGT spinterface. We notice here that the temperature dependence of the longitudinal resistance (R_{xx}) shows a metallic trend typical of FGT (Figure S3, Supporting Information).[7]

Figure 3b shows the magnetic hysteresis of a CoPc(6)/FGT(20) (thickness in nm) heterostructure measured at 10 K after FC with +10 kOe and –10 kOe, respectively. The measured hysteresis loops display a significant shift from the center (H = 0) and, in particular, a large exchange bias field H_{EB} = –840 Oe at 10 K is recorded after FC with +10 kOe (black line in Figure 3a). Here, the exchange bias field is defined as $H_{EB} = (H_{C+} + H_{C-})/2$, where H_{C+} and H_{C-} indicate the positive and negative coercive field, respectively. When we performed FC with –10 kOe and subsequently measured a Hall resistance at 10 K, the hysteresis loop shifted towards a positive field direction (red line in Figure 3a), for the same amount as in the case of the positive FC. This negative exchange bias, where the direction of a hysteresis loop shift is opposite to the direction of FC, is typically found when a ferromagnetic interfacial coupling develops at the interface between a ferromagnet and an antiferromagnet.[19]

We conducted two supplementary measurements to ensure that the measured exchange bias arises from the magnetic interaction between the layered magnetic materials and the molecular film. Firstly, we fabricated a control sample, FGT(20)/hBN without CoPc molecules, and performed the same FC procedure and AHE measurement. This control sample clearly showed a symmetric hysteresis loop without any exchange bias (Figure S4, Supporting Information). Secondly, although our CoPc/FGT structures were encapsulated by hBN in a Ar-filled glovebox, we could not ignore the possibility of oxidation during transferring the sample to the measurement chamber, which could induce the formation of an

oxidized FGT layer and exchange bias.[46] To exclude this effect, we tested a FGT(25) flake intentionally exposed to air 15 minutes without any encapsulation film. In this case, we could not detect any exchange bias nor any noticeable coercive field enhancement (Figure S5, Supporting Information).

The origin of the negative exchange bias at a CoPc/FGT interface can be understood considering that (i) the spins in the CoPc layer acquire long-range antiferromagnetic ordering and (ii) the spins of the CoPc molecules in contact to the FGT surface couple ferromagnetically to it, causing a negative shift in the hysteresis loop. This situation, which is similar to the scenario reported for other organometallic compounds on conventional magnetic materials,[27–29,49] is further validated by analyzing the temperature dependence of the exchange bias.

Figure 3c shows the AHE results measured at different temperatures from 10 K to 200 K after FC with +10 kOe. As the measurement temperature increases, the asymmetry of hysteresis loops decreases and became negligible above 80 K. From the measured loops, we collected the coercive fields and plotted them in Figure 3d and Figure S6 (Supporting Information). Compared to a control FGT device, positive coercive fields in a CoPc/FGT structure deviate significantly from the conventional exponential behavior (solid line in Figure 3d) as temperature lowers. Conversely, negative coercive fields follow well the exponential behavior (Figure S6, Supporting Information). The deviation for positive coercive fields from the exponential behavior as well as the different trend of positive and negative coercive fields confirm the presence of exchange bias. Figure 3e shows that exchange bias fields at different temperatures, collected from the data in Figure 3c, follow the exponential relation $H_{EB} = H_0 \cdot exp(-T/T_1)$, where H_0 is the extrapolated value to zero temperature and T_1 is a constant. Using this fitting, the blocking temperature (i.e. the starting point of $H_{EB} = 0$) of a CoPc(6)/FGT(20) structure is estimated as 110 K. We note that an exchange parameter corresponding to a larger

critical temperature (~ 210 K) was reported for CoPc molecules on Pb,[53] but the thickess range explored in that case (3-5 monolayers) and the reactive nature of the Pb substrate different significantly from our case. Our blocking temperature is instead analogous to that reported in other molecular exchange bias systems based on CoPc[49] and it corresponds to the estimated exchange energy for the antiferromagnetic ordering of hundreds-of-nm-thick CoPc molecular films on insulating substrates.[55] This agreement with previous results indicates that the exchange bias in FGT indeed arises from the same physical mechanism, i.e. antiferromagnetic ordering in CoPc and its interfacial coupling to FGT.

The thickness of both the ferromagnetic and the antiferromagnetic layers are critical factors determining the exchange bias. **Figure 4**a displays the hysteresis loops measured at 10 K after FC with +10 kOe in different CoPc(6)/FGT(*t*) heterostructures, in which the CoPc thickness was kept constant (6 nm) and the FGT one was varied from t = 10 nm to t = 80 nm. Here, to focus on a coercive field change, we plotted the transverse resistance R_{xy} normalized to its value at saturation. First, the coercive field increased for thinner FGT flakes. More interestingly, Figure 4b shows the dependence of the exchange bias on the FGT thickness. For thin flakes (t < 20 nm), exchange bias fields increased from H_{EB} = –62.5 Oe at 10 nm to a maximum H_{EB} = –840 Oe at 20 nm of FGT. Above 20 nm, the exchange bias field decreased gradually down to a value of H_{EB} = –145 Oe for 80 nm of FGT. In conventional exchange bias systems, the magnitude of the exchange bias is inversely proportional to the thickness of the ferromagnet as $H_{EB} \sim 1/ t_{FM}$.[19] Our CoPc(6)/FGT(*t*) system follows this relation in the FGT thickness range from 20 nm to 80 nm (red line in the inset of Figure 4b). The divergence for FGT thicknesses below 20 nm could arise from the lower volume magnetization of FGT compared to metallic ferromagnets such as Co and Fe,[7,46] which might be insufficient to fully activate the antiferromagnetic ordering in the interfacial CoPc layers. Regardless of the

thickness of FGT, all the structures exhibited negative exchange bias which highlights the favorable ferromagnetic coupling at the interface between the FGT and CoPc layers.

After having inspected the dependence of the exchange bias on the FGT thickness, we explored its change as a function of the CoPc thickness. **Figure 5**a displays the hysteresis loops measured at 10 K and after FC with +10 kOe in different CoPc(*t*)/FGT(20) heterostructures, composed of a FGT flake of 20 nm and different thicknesses of the CoPc layer (*t* = 2, 4, and 6 nm). In the same panel, we also show the hysteresis of a FGT flake directly transferred on a SiO_2 substrate without CoPc (corresponding to *t* = 0 nm), which displays a coercive field of approximately 3 kOe without exchange bias. For the FGT flake on the 2-nm-thick CoPc layer, we observed a finite exchange bias and a larger coercive field. A similar increase in coercive field is often observed for ferromagnet/antiferromagnet structures characterized by inhomogeneous magnetic textures at the interface.[63,64] Following the same tendency, an even larger coercive field was recorded for a FGT flake on the 4-nm-thick CoPc layer, which was also characterized by a larger exchange bias field. Finally, we found a maximum exchange bias field and a reduced coercive field for the CoPc thickness of 6 nm. We understand this finding considering that while the 2- and 4-nm-thick CoPc films do not form continuous films, the 6-nm-thick CoPc film forms a homogeneous interface with FGT, pinning more efficiently the FGT magnetization (see Figure S7, Supporting Information).

Figure 5b displays the increase in an exchange bias field with a CoPc thickness from H_{EB} = 0 Oe (without CoPc) to H_{EB} = –840 Oe (at CoPc 6 nm).

Furthermore, the quality of a magnetic heterointerface at a ferromagnet/antiferromagnet structure can be evaluated by the ratio between the exchange bias and the coercive field (H_{EB}/H_C).[63,64] Therefore, Figure 5b also shows the H_{EB}/H_C ratio in the CoPc(*t*)/FGT(20) structures. The H_{EB}/H_C ratio reaches a remarkably large value of 0.34, corresponding to the

CoPc thickness of 6 nm. This value is the highest among the reported exchange bias structures based on FGT (see Table S1 for comparison with other systems),[13–16,46,47] indicating the high quality of the magnetic CoPc/FGT spinterface.

3. Conclusion

In this study, we demonstrated the emergence of spinterface effects in hybrid van der Waals heterostructures composed of a CoPc film interfaced with a flake of a layered ferromagnet FGT. The formation of a homogeneous CoPc layer and of a flat and sharp CoPc/FGT interface, confirmed through micro-Raman spectroscopy and STEM, are ideal for the emergence of magnetic interaction between the unpaired spins in CoPc and the ferromagnetic FGT. Magnetotransport measurements performed following a FC procedure indicate that the interfacial magnetic interaction induces exchange bias in FGT persisting up to 110 K. This blocking temperature is analogous to the reported exchange energy of antiferromagnetic ordering of CoPc layers,[49,55] suggesting that the CoPc layer develops antiferromagnetic ordering which couples ferromagnetically to the FGT surface, pinning its magnetization. This is corroborated by analyzing the AHE of CoPc/FGT heterostructures with different CoPc thicknesses, which evolve from an increase in coercive field for thin CoPc layers to a fully developed exchange bias for thicker layers. The H_{EB} = –840 Oe at 10 K, recorded for a 20-nm-thick FGT flake, is the strongest value reported so far for layered magnetic materials, highlighting the superior quality of the CoPc/FGT spinterface. In perspective, an improved control over other interfacial effects, such as charge transfer or dipolar interaction, may enable the design of new functional interfaces with enhanced magnetic interactions. Our results show that hybrid van der Waals heterostructures composed of layered magnetic material interfaced to organic molecules represent an ideal materials platform to develop high quality spinterface

effects, which would be a key element in atomically precise multifunctional structures for practical device application.

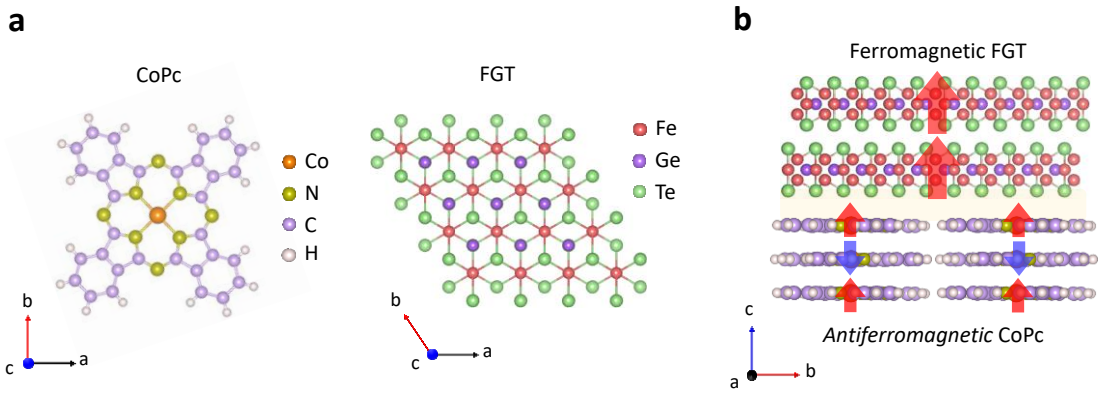

Figure 1. Schematics of a hybrid van der Waals heterostructure resulting from interfacing CoPc and FGT. a) Chemical structures of a planar molecule CoPc and of a layered ferromagnet FGT (top view). b) Schematic rendering of a hybrid CoPc/FGT heterostructure (lateral view). The emerging spinterface mechanism is also sketched: the ferromagnetic FGT flake (red arrows in the picture) interfaced with the CoPc layers activate their antiferromagnetic molecular ordering (red/blue arrows), which in turn pins the FGT magnetization introducing exchange bias.

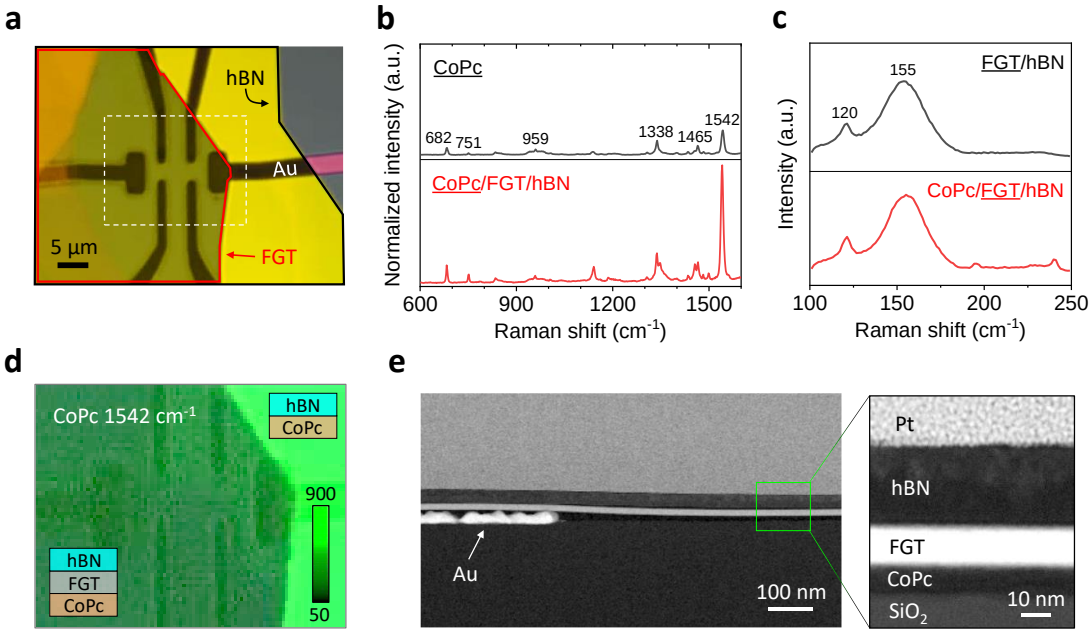

Figure 2. Structural characterization of a hybrid CoPc/FGT heterostructure. a) Optical image of a CoPc/FGT structure encapsulated by hBN. The CoPc layers cover all the substrate area in this image, and the red and black lines indicate the FGT and hBN flakes, respectively. b) Representative Raman spectra for CoPc films covered by FGT/hBN (bottom) or in an exposed region (top). The spectra are normalized to the intensity of the Si peak at 520 cm^{-1}. c) Representative Raman spectra for FGT with and without CoPc layers. The typical FGT peaks at 120 cm^{-1} and 155 cm^{-1} appear unaltered in both FGT/hBN and CoPc/FGT/hBN structures. d) Raman map image for CoPc (1542 cm^{-1}) in the white dotted line region of Figure 2a, displaying the formation of a homogeneous CoPc molecular layer. The region covered by FGT shows a lower Raman intensity due to the light absorbance from the FGT flake. The Raman spectra were acquired using an 532-nm excitation laser. e) Cross-sectional STEM images of a CoPc/FGT/hBN structure. The interface is flat and homogeneous.

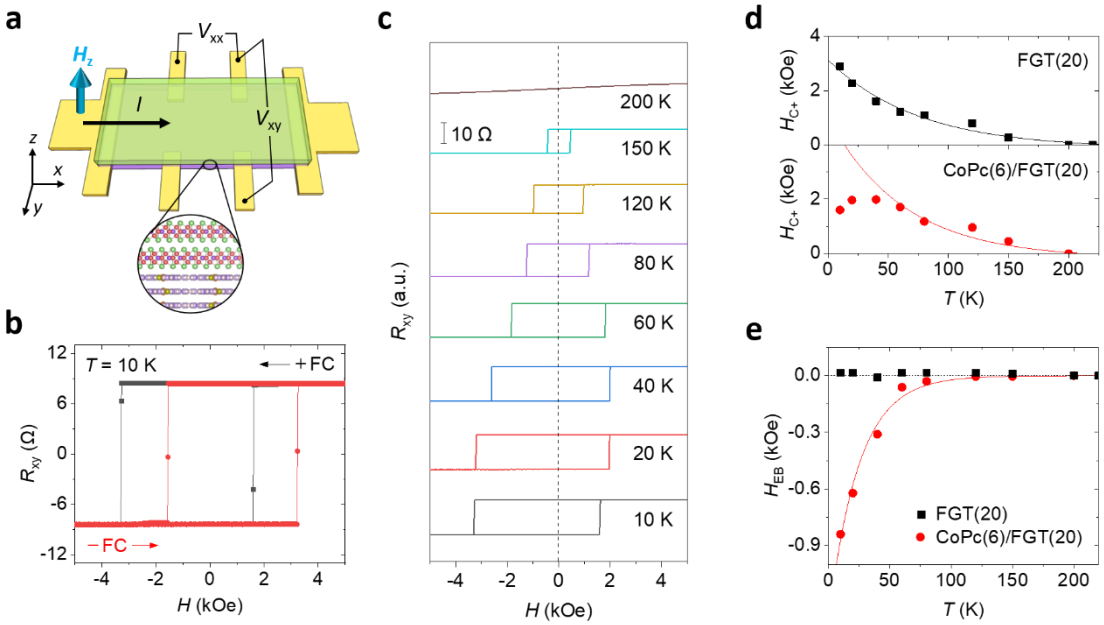

Figure 3. Exchange bias in a CoPc(6)/FGT(20) heterostructure. The numbers between parenthesis indicate the thickness in nanometers. a) Sketch of a CoPc/FGT device. An electrical current (I) is applied along the longitudinal direction (x) and the Hall voltage (V_{xy}) is measured transversally (along y) while applying an out-of-plane magnetic field (along z). b) Hall resistance as a function of the magnetic field at 10 K after FC with +10 kOe (+FC) and –10 kOe (–FC). The hysteresis associated to the AHE of the FGT, is shifted to the opposite directions with respect to the polarity of the FC, and the magnitude of these shifts is identical. c) Temperature-dependent AHE after FC with +10 kOe. The asymmetry of a hysteresis loop decreases as temperature increases. d) Temperature-dependence of a positive coercive field, H_{C+}, after FC with +10 kOe in a FGT(20) and CoPc(6)/FGT(20) structure. The control sample of FGT displays an exponential increase of H_{C+} when lowering temperature, while the CoPc/FGT heterostructure displays a deviation from the exponential trend at low temperatures, where the exchange bias emerges. e) Exchange bias fields, H_{EB}, as a function of temperature in a CoPc(6)/FGT(20) and in a FGT(20) structure. The exchange bias in the

CoPc/FGT follows an exponential behavior with an estimated blocking temperature of 110 K.

No exchange bias is recorded in the control sample of FGT.

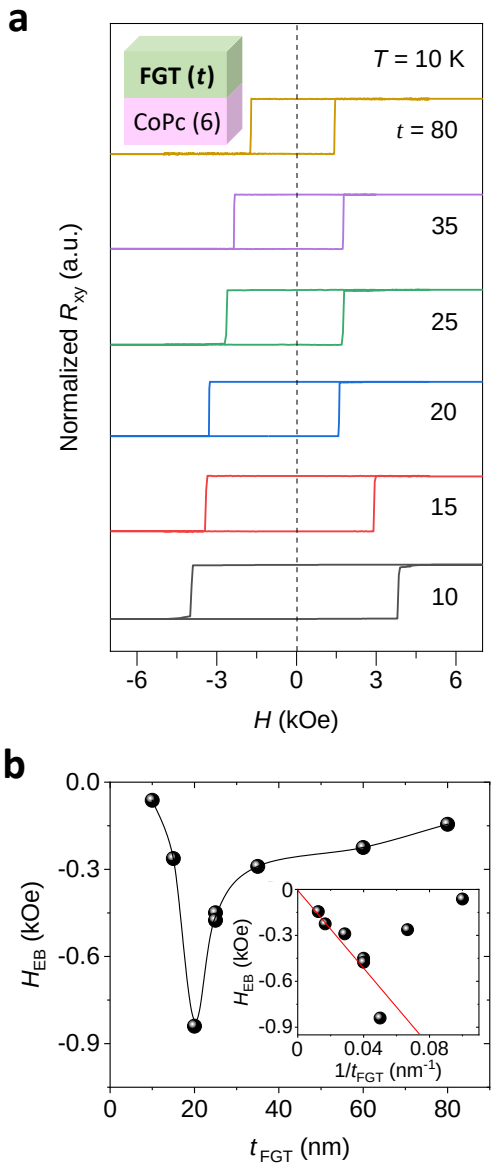

Figure 4. Dependence of exchange bias on the FGT thickness. a) AHE measured in different CoPc(6)/FGT(*t*) heterostructures composed of a 6-nm-thick CoPc film and a FGT flake with varying thickness (between 10 and 80 nm). b) Dependence of the exchange bias field in the CoPc(6)/FGT(*t*) heterostructures as a function of the FGT thickness t_{FGT}, as extracted from the curves in (a). Inset: the same data plotted as a function of $1/t_{FGT}$ highlights the proportional relation between H_{EB} with the inverse of the FGT thickness from 20 nm to 80 nm. These data were measured at 10 K after a FC procedure with +10 kOe.

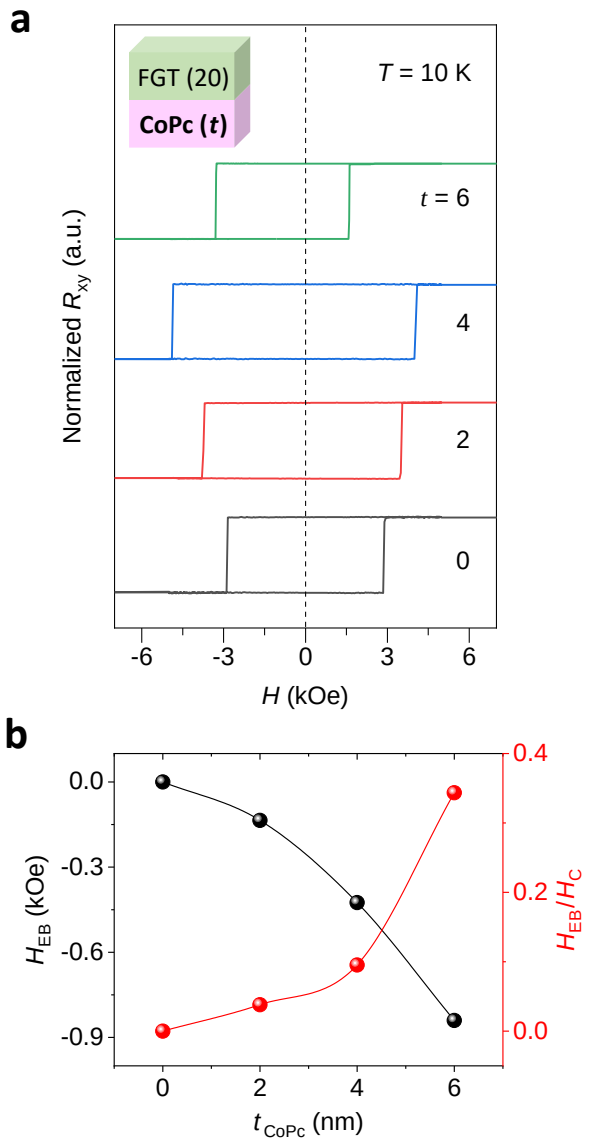

Figure 5. Dependence of exchange bias on the CoPc thickness. a) AHE measured in different CoPc(*t*)/FGT(20) heterostructures composed of a 20-nm-thick FGT flake and a CoPc film of varying thickness (between 0 and 6 nm, where 0 nm corresponds to the absence of CoPc. b) Dependence of H_{EB} in CoPc(*t*)/FGT(20) heterostructures as a function of the CoPc thickness t_{CoPc}, as extracted from the curves in (a). The H_{EB}/H_C ratio is also shown, where H_C is a coercive field in the measured hysteresis, recorded as a half of the loop width.

Experimental Section/Methods

Sample preparation: Ti/Au electrodes (2+10 nm) with a Hall-bar geometry were prepatterned on a Si/SiO_2 substrate. The channel dimension in the Hall pattern is 10 μm x 2 μm. CoPc molecules (purchased from Sigma Aldrich) were deposited on the electrode-prepatterned Si/SiO_2 substrates, previously cleaned with acetone, isopropyl alcohol, and plasma treatment. The deposition rate of CoPc was controlled to 0.1 Å/s while the substrate was maintained at room temperature, and the base pressure of vacuum was 1.2×10^{-8} mbar. A FGT flake (HQ graphene) was prepared by mechanical exfoliation using a blue tape (Nitto® SPV224) and transferred to a PDMS film (Gel-pak). The thickness of an exfoliated FGT flake on a PDMS film was characterized by optical contrast in an optical microscope, and confirmed again by using atomic force microscopy (Agilent 5500 SPM). The selected FGT flake was transferred onto the electrode-prepatterned substrate and encapsulated by a hBN flake as the same way. Exfoliation and stamping were performed in an Ar-filled glovebox (H_2O and O_2 < 0.1 ppm). The device fabrication employed in this study is very reproducible and the presence of the CoPc thin film did not worsen the electrical contact. The devices in which the stamping process was successful (no misalignment, no damage to the flake) reproducibly displayed linear *I-V* characteristics with low contact resistance (in the range 1 kΩ - 2 kΩ), whereas the four-probe resistance was typically in the 50 Ω - 200 Ω range for 20-nm-thick FGT flakes.

Raman characterization: Micro-Raman measurements (Renishaw InVia Qontor micro-Raman instrument) were carried out at room temperature using a 100× objective with a sample kept in high vacuum in a Linkam chamber. The 532 nm and 633 nm laser excitation sources were used, as stated in each case. A step (*x*,*y*) size of 0.2 μm x 0.2 μm was used for micro-Raman mapping.

TEM analysis: STEM data was acquired using TitanG2 60-300 electron microscope (FEI, Netherlands) equipped with xFEG, monochromator, image aberration corrector, HAADF STEM detector, and Quantum GIF (Gatan, UK). Images were obtained at 300 kV accelerating voltage. Cross-section samples of the devices have been prepared by a standard FIB protocol using Helios 600 FIB/SEM (FEI, Netherlands).

Magnetotransport measurement: Electrical transport measurements were performed in a physical property measurement system (PPMS, Quantum Design) with a rotational sample stage. An electrical current was applied by a Keithley 6221 and a measured voltage was detected by a Keithley 2182 nanovoltmeter. For a FC procedure, the magnetic field of ±10 kOe was applied at 300 K and a sample was cooled down to a low temperature (10 K) while maintaining the magnetic field. The measurement with a magnetic field sweep started from the applied magnetic field (±10 kOe).

Supporting Information

Supporting Information is available from the Wiley Online Library or from the author.

Acknowledgements

This work is supported by “la Caixa” Foundation (ID 100010434), under the agreement LCF/BQ/PI19/11690017, by the Spanish MICINN under Project PID2019-108153GA-I00, RTI2018-094861-B-100 and under the María de Maeztu Units of Excellence Program (MDM-2016-0618). B.M-G. thanks Gipuzkoa Council (Spain) in the frame of Gipuzkoa Fellows Program. J. J. acknowledges the support of Basic Science Research Program through the National Research Foundation of Korea (NRF) funded by the Ministry of Education (2020R1A6A3A03039086).

Received: ((will be filled in by the editorial staff))
Revised: ((will be filled in by the editorial staff))
Published online: ((will be filled in by the editorial staff))

References

[1] B. Huang, G. Clark, E. Navarro-Moratalla, D. R. Klein, R. Cheng, K. L. Seyler, D. Zhong, E. Schmidgall, M. A. McGuire, D. H. Cobden, W. Yao, D. Xiao, P. Jarillo-Herrero, X. Xu, *Nature* **2017**, *546*, 270.

[2] C. Gong, L. Li, Z. Li, H. Ji, A. Stern, Y. Xia, T. Cao, W. Bao, C. Wang, Y. Wang, Z. Q. Qiu, R. J. Cava, S. G. Louie, J. Xia, X. Zhang, *Nature* **2017**, *546*, 265.

[3] C. Gong, X. Zhang, *Science* **2019**, *363*, eaav4450.

[4] M. Gibertini, M. Koperski, A. F. Morpurgo, K. S. Novoselov, *Nat. Nanotechnol.* **2019**, *14*, 408.

[5] J. Chu, Y. Wang, X. Wang, K. Hu, G. Rao, C. Gong, C. Wu, H. Hong, X. Wang, K. Liu, C. Gao, J. Xiong, *Adv. Mater.* **2021**, *33*, 2004469.

[6] M. Serri, G. Cucinotta, L. Poggini, G. Serrano, P. Sainctavit, J. Strychalska-Nowak, A. Politano, F. Bonaccorso, A. Caneschi, R. J. Cava, R. Sessoli, L. Ottaviano, T. Klimczuk, V. Pellegrini, M. Mannini, *Adv. Mater.* **2020**, *32*, 2000566.

[7] Z. Fei, B. Huang, P. Malinowski, W. Wang, T. Song, J. Sanchez, W. Yao, D. Xiao, X. Zhu, A. F. May, W. Wu, D. H. Cobden, J.-H. Chu, X. Xu, *Nat. Mater.* **2018**, *17*, 778.

[8] K. Kim, J. Seo, E. Lee, K. T. Ko, B. S. Kim, B. G. Jang, J. M. Ok, J. Lee, Y. J. Jo, W. Kang, J. H. Shim, C. Kim, H. W. Yeom, B. Il Min, B.-J. Yang, J. S. Kim, *Nat. Mater.* **2018**, *17*, 794.

[9] W. Zhu, H. Lin, F. Yan, C. Hu, Z. Wang, L. Zhao, Y. Deng, Z. R. Kudrynskyi, T. Zhou, Z. D. Kovalyuk, Y. Zheng, A. Patanè, I. Žutić, S. Li, H. Zheng, K. Wang, *Adv. Mater.* **2021**, *33*, 2104658.

[10] X. Chen, H. Wang, H. Liu, C. Wang, G. Wei, C. Fang, H. Wang, C. Geng, S. Liu, P. Li, H. Yu, W. Zhao, J. Miao, Y. Li, L. Wang, T. Nie, J. Zhao, X. Wu, *Adv. Mater.* **2022**, *34*, 2106172.

[11] Y. Deng, Y. Yu, Y. Song, J. Zhang, N. Z. Wang, Z. Sun, Y. Yi, Y. Z. Wu, S. Wu, J. Zhu, J. Wang, X. H. Chen, Y. Zhang, *Nature* **2018**, *563*, 94.

[12] K. Zhang, S. Han, Y. Lee, M. J. Coak, J. Kim, I. Hwang, S. Son, J. Shin, M. Lim, D. Jo, K. Kim, D. Kim, H. Lee, J. Park, *Adv. Mater.* **2021**, *33*, 2004110.

[13] G. Hu, Y. Zhu, J. Xiang, T.-Y. Yang, M. Huang, Z. Wang, Z. Wang, P. Liu, Y. Zhang, C. Feng, D. Hou, W. Zhu, M. Gu, C.-H. Hsu, F.-C. Chuang, Y. Lu, B. Xiang, Y.-L. Chueh, *ACS Nano* **2020**, *14*, 12037.

[14] L. Zhang, X. Huang, H. Dai, M. Wang, H. Cheng, L. Tong, Z. Li, X. Han, X. Wang, L. Ye, J. Han, *Adv. Mater.* **2020**, *32*, 2002032.

[15] R. Zhu, W. Zhang, W. Shen, P. K. J. Wong, Q. Wang, Q. Liang, Z. Tian, Y. Zhai, C. Qiu, A. T. S. Wee, *Nano Lett.* **2020**, *20*, 5030.

[16] H. Dai, H. Cheng, M. Cai, Q. Hao, Y. Xing, H. Chen, X. Chen, X. Wang, J.-B. Han, *ACS Appl. Mater. Interfaces* **2021**, *13*, 24314.

[17] I. Žutić, A. Matos-Abiague, B. Scharf, H. Dery, K. Belashchenko, *Mater. Today* **2019**, *22*, 85.

[18] M. Ali, P. Adie, C. H. Marrows, D. Greig, B. J. Hickey, R. L. Stamps, *Nat. Mater.* **2007**, *6*, 70.

[19] J. Nogués, I. K. Schuller, *J. Magn. Magn. Mater.* **1999**, *192*, 203.

[20] F. Hellman, A. Hoffmann, Y. Tserkovnyak, G. S. D. Beach, E. E. Fullerton, C. Leighton, A. H. MacDonald, D. C. Ralph, D. A. Arena, H. A. Dürr, P. Fischer, J. Grollier, J. P. Heremans, T. Jungwirth, A. V. Kimel, B. Koopmans, I. N. Krivorotov, S. J. May, A. K.

Petford-Long, J. M. Rondinelli, N. Samarth, I. K. Schuller, A. N. Slavin, M. D. Stiles, O. Tchernyshyov, A. Thiaville, B. L. Zink, *Rev. Mod. Phys.* **2017**, *89*, 025006.

[21] S. Sanvito, *Nat. Phys.* **2010**, *6*, 562.

[22] M. Cinchetti, V. A. Dediu, L. E. Hueso, *Nat. Mater.* **2017**, *16*, 507.

[23] H. Wende, M. Bernien, J. Luo, C. Sorg, N. Ponpandian, J. Kurde, J. Miguel, M. Piantek, X. Xu, P. Eckhold, W. Kuch, K. Baberschke, P. M. Panchmatia, B. Sanyal, P. M. Oppeneer, O. Eriksson, *Nat. Mater.* **2007**, *6*, 516.

[24] S. Javaid, M. Bowen, S. Boukari, L. Joly, J.-B. Beaufrand, X. Chen, Y. J. Dappe, F. Scheurer, J.-P. Kappler, J. Arabski, W. Wulfhekel, M. Alouani, E. Beaurepaire, *Phys. Rev. Lett.* **2010**, *105*, 077201.

[25] A. Lodi Rizzini, C. Krull, T. Balashov, J. J. Kavich, A. Mugarza, P. S. Miedema, P. K. Thakur, V. Sessi, S. Klyatskaya, M. Ruben, S. Stepanow, P. Gambardella, *Phys. Rev. Lett.* **2011**, *107*, 177205.

[26] K. V. Raman, A. M. Kamerbeek, A. Mukherjee, N. Atodiresei, T. K. Sen, P. Lazić, V. Caciuc, R. Michel, D. Stalke, S. K. Mandal, S. Blügel, M. Münzenberg, J. S. Moodera, *Nature* **2013**, *493*, 509.

[27] M. Gruber, F. Ibrahim, S. Boukari, H. Isshiki, L. Joly, M. Peter, M. Studniarek, V. Da Costa, H. Jabbar, V. Davesne, U. Halisdemir, J. Chen, J. Arabski, E. Otero, F. Choueikani, K. Chen, P. Ohresser, W. Wulfhekel, F. Scheurer, W. Weber, M. Alouani, E. Beaurepaire, M. Bowen, *Nat. Mater.* **2015**, *14*, 981.

[28] J. Jo, J. Byun, I. Oh, J. Park, M. J. Jin, B. C. Min, J. Lee, J. W. Yoo, *ACS Nano* **2019**, *13*, 894.

[29] J. Jo, J. Byun, J. Lee, D. Choe, I. Oh, J. Park, M.-J. Jin, J. Lee, J.-W. Yoo, *Adv. Funct. Mater.* **2020**, *30*, 1908499.

[30] S. Miwa, K. Kondou, S. Sakamoto, A. Nihonyanagi, F. Araoka, Y. Otani, D. Miyajima, *Appl. Phys. Express* **2020**, *13*, 113001.

[31] C. Barraud, P. Seneor, R. Mattana, S. Fusil, K. Bouzehouane, C. Deranlot, P. Graziosi, L. Hueso, I. Bergenti, V. Dediu, F. Petroff, A. Fert, *Nat. Phys.* **2010**, *6*, 615.

[32] D. Ciudad, M. Gobbi, C. J. Kinane, M. Eich, J. S. Moodera, L. E. Hueso, *Adv. Mater.* **2014**, *26*, 7561.

[33] K. Bairagi, A. Bellec, V. Repain, C. Chacon, Y. Girard, Y. Garreau, J. Lagoute, S. Rousset, R. Breitwieser, Y.-C. Hu, Y. C. Chao, W. W. Pai, D. Li, A. Smogunov, C. Barreteau, *Phys. Rev. Lett.* **2015**, *114*, 247203.

[34] S. Vélez, D. Ciudad, J. Island, M. Buscema, O. Txoperena, S. Parui, G. A. Steele, F. Casanova, H. S. J. van der Zant, A. Castellanos-Gomez, L. E. Hueso, *Nanoscale* **2015**, *7*, 15442.

[35] S. Parui, L. Pietrobon, D. Ciudad, S. Vélez, X. Sun, F. Casanova, P. Stoliar, L. E. Hueso, *Adv. Funct. Mater.* **2015**, *25*, 2972.

[36] A. Koma, *Thin Solid Films* **1992**, *216*, 72.

[37] Y.-J. Yu, G.-H. Lee, J. I. Choi, Y. S. Shim, C.-H. Lee, S. J. Kang, S. Lee, K. T. Rim, G. W. Flynn, J. Hone, Y.-H. Kim, P. Kim, C. Nuckolls, S. Ahn, *Adv. Mater.* **2017**, *29*, 1603925.

[38] M. Gobbi, S. Bonacchi, J. X. Lian, A. Vercouter, S. Bertolazzi, B. Zyska, M. Timpel, R. Tatti, Y. Olivier, S. Hecht, M. V. Nardi, D. Beljonne, E. Orgiu, P. Samorì, *Nat. Commun.* **2018**, *9*, 2661.

[39] M. Gobbi, S. Bonacchi, J. X. Lian, Y. Liu, X.-Y. Wang, M.-A. Stoeckel, M. A. Squillaci, G. D'Avino, A. Narita, K. Müllen, X. Feng, Y. Olivier, D. Beljonne, P. Samorì, E. Orgiu, *Nat. Commun.* **2017**, *8*, 14767.

[40] F. Calavalle, P. Dreher, A. P. Surdendran, W. Wan, M. Timpel, R. Verucchi, C. Rogero, T. Bauch, F. Lombardi, F. Casanova, M. V. Nardi, M. M. Ugeda, L. E. Hueso, M. Gobbi, *Nano Lett.* **2021**, *21*, 136.

[41] D. Jariwala, T. J. Marks, M. C. Hersam, *Nat. Mater.* **2017**, *16*, 170.

[42] M. Gobbi, E. Orgiu, P. Samori, *Adv. Mater.* **2018**, *30*, 1706103.

[43] L. Daukiya, J. Seibel, S. De Feyter, *Adv. Phys.: X* **2019**, *4*, 1625723.

[44] R. Torres-Cavanillas, M. Morant-Giner, G. Escorcia-Ariza, J. Dugay, J. Canet-Ferrer, S. Tatay, S. Cardona-Serra, M. Giménez-Marqués, M. Galbiati, A. Forment-Aliaga, E. Coronado, *Nat. Chem.* **2021**, *13*, 1101.

[45] Y. Zhao, M. Gobbi, L. E. Hueso, P. Samorì, *Chem. Rev.* **2022**, *122*, 50.

[46] H. K. Gweon, S. Y. Lee, H. Y. Kwon, J. Jeong, H. J. Chang, K.-W. Kim, Z. Q. Qiu, H. Ryu, C. Jang, J. W. Choi, *Nano Lett.* **2021**, *21*, 1672.

[47] Y. Zhang, H. Xu, C. Yi, X. Wang, Y. Huang, J. Tang, J. Jiang, C. He, M. Zhao, T. Ma, J. Dong, C. Guo, J. Feng, C. Wan, H. Wei, H. Du, Y. Shi, G. Yu, G. Zhang, X. Han, *Appl. Phys. Lett.* **2021**, *118*, 262406.

[48] G. Zheng, W.-Q. Xie, S. Albarakati, M. Algarni, C. Tan, Y. Wang, J. Peng, J. Partridge, L. Farrar, J. Yi, Y. Xiong, M. Tian, Y.-J. Zhao, L. Wang, *Phys. Rev. Lett.* **2020**, *125*, 047202.

[49] S. Boukari, H. Jabbar, F. Schleicher, M. Gruber, G. Avedissian, J. Arabski, V. Da Costa, G. Schmerber, P. Rengasamy, B. Vileno, W. Weber, M. Bowen, E. Beaurepaire, *Nano Lett.* **2018**, *18*, 4659.

[50] H. Isshiki, K. Kondou, S. Takizawa, K. Shimose, T. Kawabe, E. Minamitani, N. Yamaguchi, F. Ishii, A. Shiotari, Y. Sugimoto, S. Miwa, Y. Otani, *Nano Lett.* **2019**, *19*, 7119.

[51] C. G. Claessens, U. Hahn, T. Torres, *Chem. Record* **2008**, *8*, 75.

[52] A. Mugarza, R. Robles, C. Krull, R. Korytár, N. Lorente, P. Gambardella, *Phys. Rev. B* **2012**, *85*, 155437.

[53] X. Chen, Y.-S. Fu, S.-H. Ji, T. Zhang, P. Cheng, X.-C. Ma, X.-L. Zou, W.-H. Duan, J.-F. Jia, Q.-K. Xue, *Phys. Rev. Lett.* **2008**, *101*, 197208.

[54] W. Wu, N. M. Harrison, A. J. Fisher, *Phys. Rev. B* **2013**, *88*, 024426.

[55] M. Serri, W. Wu, L. R. Fleet, N. M. Harrison, C. F. Hirjibehedin, C. W. Kay, A. J. Fisher, G. Aeppli, S. Heutz, *Nat. Commun.* **2014**, *5*, 3079.

[56] T. V. Basova, V. G. Kiselev, B.-E. Schuster, H. Peisert, T. Chasse, *J. Raman Spectrosc.* **2009**, *40*, 2080.

[57] S. Heutz, S. M. Bayliss, R. L. Middleton, G. Rumbles, T. S. Jones, *J. Phys. Chem. B* **2000**, *104*, 7124.

[58] A. Kumar, D. Naumenko, L. Cozzarini, L. Barba, A. Cassetta, M. Pedio, *J. Raman Spectrosc.* **2018**, *49*, 1015.

[59] X. Ling, L. Xie, Y. Fang, H. Xu, H. Zhang, J. Kong, M. S. Dresselhaus, J. Zhang, Z. Liu, *Nano Lett.* **2010**, *10*, 553.

[60] S. Huang, X. Ling, L. Liang, Y. Song, W. Fang, J. Zhang, J. Kong, V. Meunier, M. S. Dresselhaus, *Nano Lett.* **2015**, *15*, 2892.

[61] X. Ling, J. Wu, W. Xu, J. Zhang, *Small* **2012**, *8*, 1365.

[62] L. Du, J. Tang, Y. Zhao, X. Li, R. Yang, X. Hu, X. Bai, X. Wang, K. Watanabe, T. Taniguchi, D. Shi, G. Yu, X. Bai, T. Hasan, G. Zhang, Z. Sun, *Adv. Funct. Mater.* **2019**, *29*, 1904734.

[63] M. D. Stiles, R. D. McMichael, *Phys. Rev. B* **2001**, *63*, 064405.

[64] K. O'Grady, L. E. Fernandez-Outon, G. Vallejo-Fernandez, *J. Magn. Magn. Mater.* **2010**, *322*, 883.

The table of contents

Exchange bias in molecule/Fe_3GeTe_2 van der Waals heterostructures via spinterface effects

Junhyeon Jo, Francesco Calavalle, Beatriz Martín-García, Daniel Tezze, Felix Casanova, Andrey Chuvilin, Luis E. Hueso*, and Marco Gobbi**

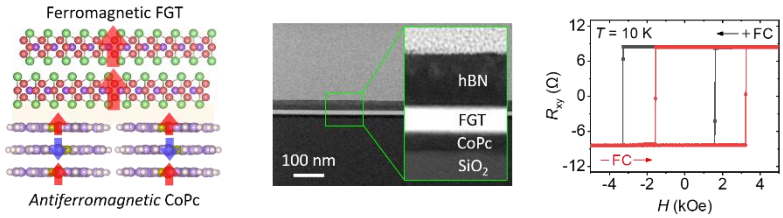

Spinterface effects are demonstrated in a hybrid van der Waals heterostructure composed of a CoPc film interfaced with a layered ferromagnet Fe_3GeTe_2. The interface interactions introduce an exchange bias field in Fe_3GeTe_2, which is among the strongest reported for layered magnetic materials. Our results demonstrate the potential of molecular functionalization for tailoring the magnetic properties of layered materials.

Supporting Information

Exchange bias in molecule/Fe_3TeGe_2 van der Waals heterostructures via spinterface effects

Junhyeon Jo, Francesco Calavalle, Beatriz Martín-García, Daniel Tezze, Felix Casanova, Andrey Chuvilin, Luis E. Hueso*, and Marco Gobbi**

a

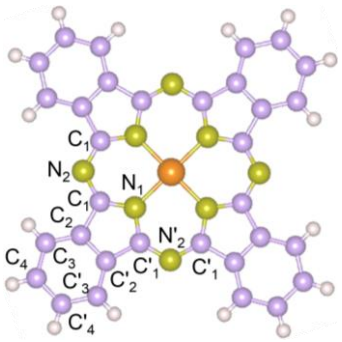

b

Wavenumber	Symmetry	Assignments
1542 cm^{-1}	B_{1g}	C_1-N_2
1465 cm^{-1}	B_{1g}	C_2-C_2, C_2-C_3-H
	B_{2g}	C_1-N_2, N_1-C_1-C_2, C-C-H
1338 cm^{-1}	B_{1g}	C_2-C_2, C_1-C_2-C_2, C_3-C_4, C_2-C_3
1308 cm^{-1}	B_{1g}	C_1-N_1, C_1-N_1-C_1
	B_{2g}	C_2-C_3-H, C_3-C_4-H
959 cm^{-1}	B_{2g}	N_1-Co-N_1, C_1-N_2-C_1, C_2-C_1-N_2
	E_g	C_3-C_4-H, C_4-C_4-H
751 cm^{-1}	B_{1g}	Co-N_1, C_1-N_1-C_1, N_2-C_1-C_2
	E_g	C_3-C_4-H, C_2-C_3-H
682 cm^{-1}	A_{1g}	C_1-N_2-C_1, N_1-C_1, N_1-C_1-C_2
	B_{2g}	C_1-C_2-C_3

c

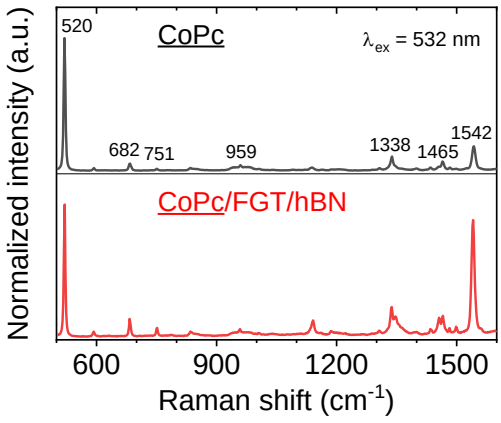

d

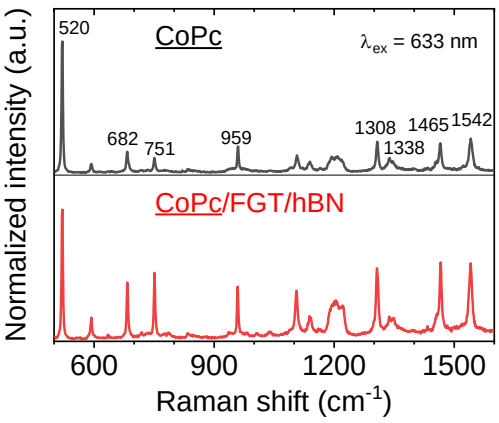

Figure S1. Raman characterization of CoPc. a) The structure and atomic notation of a CoPc molecule. b) Details about intra-bonding and symmetry for CoPc Raman peaks.[56] All the Raman spectra of the CoPc show identical features to the CoPc in the heterostructure of CoPc/FGT/hBN in Figure 2b. c),d) Representative Raman spectra for CoPc films covered by FGT/hBN (bottom) or left uncovered (top). The spectra are normalized to the intensity of the Si peak at 520 cm^{-1}. These spectra in (c) and (d) were acquired using a 532-nm and a 633-nm excitation laser, respectively. For the spectra in (c), which are those shown in Figure 2b of the main text, we display here the full measurement range, including the Si peak at 520 cm^{-1} used for the normalization. In (c) and (d), we observe an increase in the intensity of the molecular modes in the region below FGT.

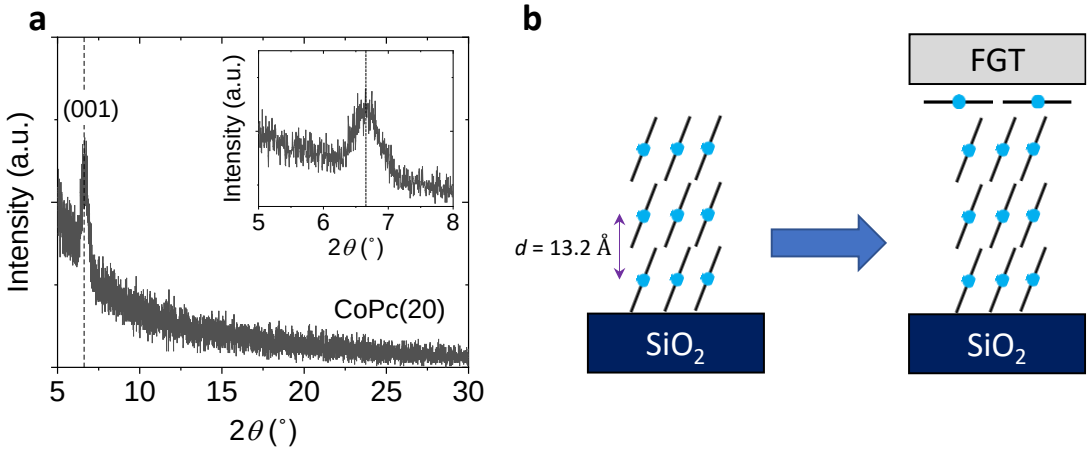

Figure S2. X-ray diffractometry for CoPc. (a) X-ray diffraction pattern measured on a 20-nm-thick CoPc layer. A single peak is observed at 6.7°, which corresponds to CoPc molecules arranged in the α-phase with the (001) molecular plane parallel to the SiO_2 substrate surface. (b) A simplified sketch of the molecular arrangement in our CoPc films. CoPc molecules are displayed in a side-view with the central Co atoms represented in light blue and the organic ligands as black lines. Our films are in the α-phase with the (001) molecular plane parallel to the SiO_2 substrate surface. The stamping of the FGT flake introduces a rearrangement of the uppermost molecular layer, where molecules tilt to lie parallel to the FGT surface. This local rearrangement can be understood considering that Pc molecules possess a high affinity to the basal plane of van der Waals materials. Indeed, when deposited on graphitic surfaces, they typically lie flat to maximize the van der Waals interaction with the surface. While stamping the flake onto the molecular film is certainly a different situation, the mechanical pressure exerted by the van der Waals surface and the thermal energy leads to the energetically favored configuration in which the molecules lie flat at the interface, and parallel to the FGT surface.

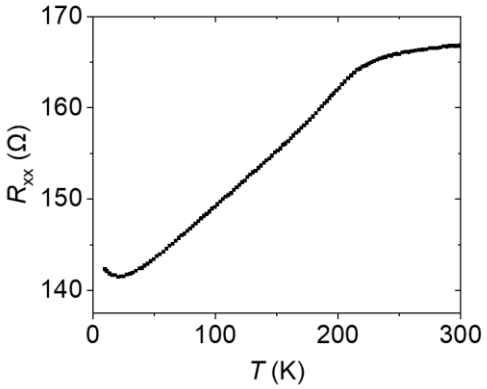

Figure S3. Temperature-dependent longitudinal resistance of a CoPc(6)/FGT(20) heterostructure. A kink near 200 K indicates the phase transition of FGT from paramagnetism to ferromagnetism.

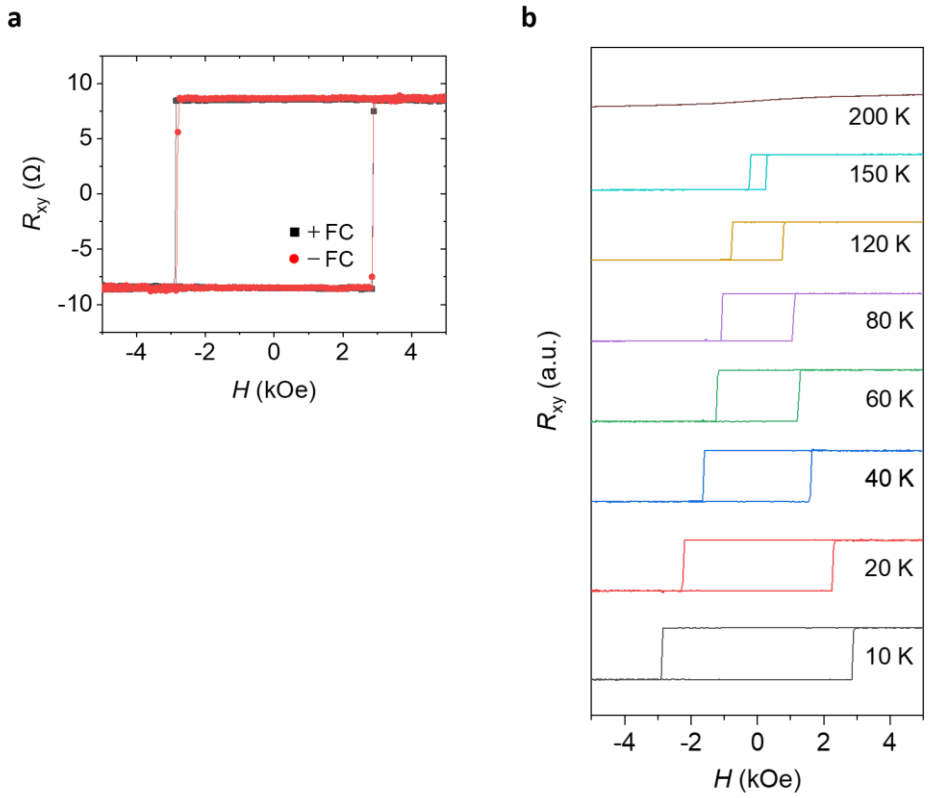

Figure S4. AHE measurement on a hBN-capped FGT(20) structure after a FC procedure. a) Hysteresis loop measured at 10 K after FC with ±10 kOe. Without CoPc layers, we found no asymmetry at a positive and negative coercive field. b) AHE measured at different temperatures from 10 K to 200 K after FC with +10 kOe. Exchange bias is not observed in any of the loops.

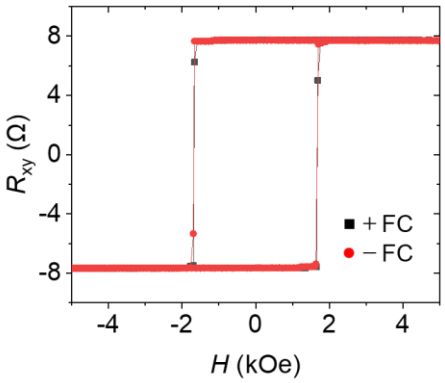

Figure S5. AHE measurement on a FGT(25)/O-FGT(*x*) structure at 10 K after FC with ±10 kOe. There is no signature of exchange bias even though an exfoliated 25-nm-thick FGT flake was intentionally exposed to air 15 mins before encapsulated by hBN.

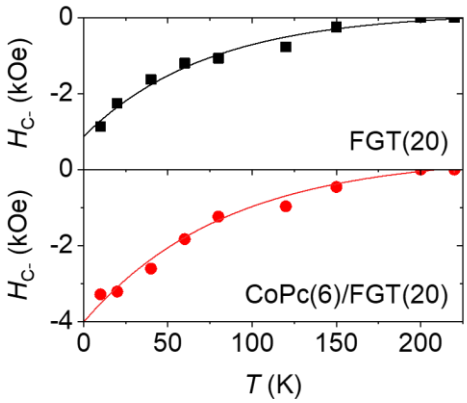

Figure S6. Temperature-dependence of a negative coercive field, H_{C-}, after FC with +10 kOe in a FGT(20) and CoPc(6)/FGT(20) structure. Both the control sample of FGT and the CoPc/FGT heterostructure display an exponential behavior of H_{C-} on varying temperature.

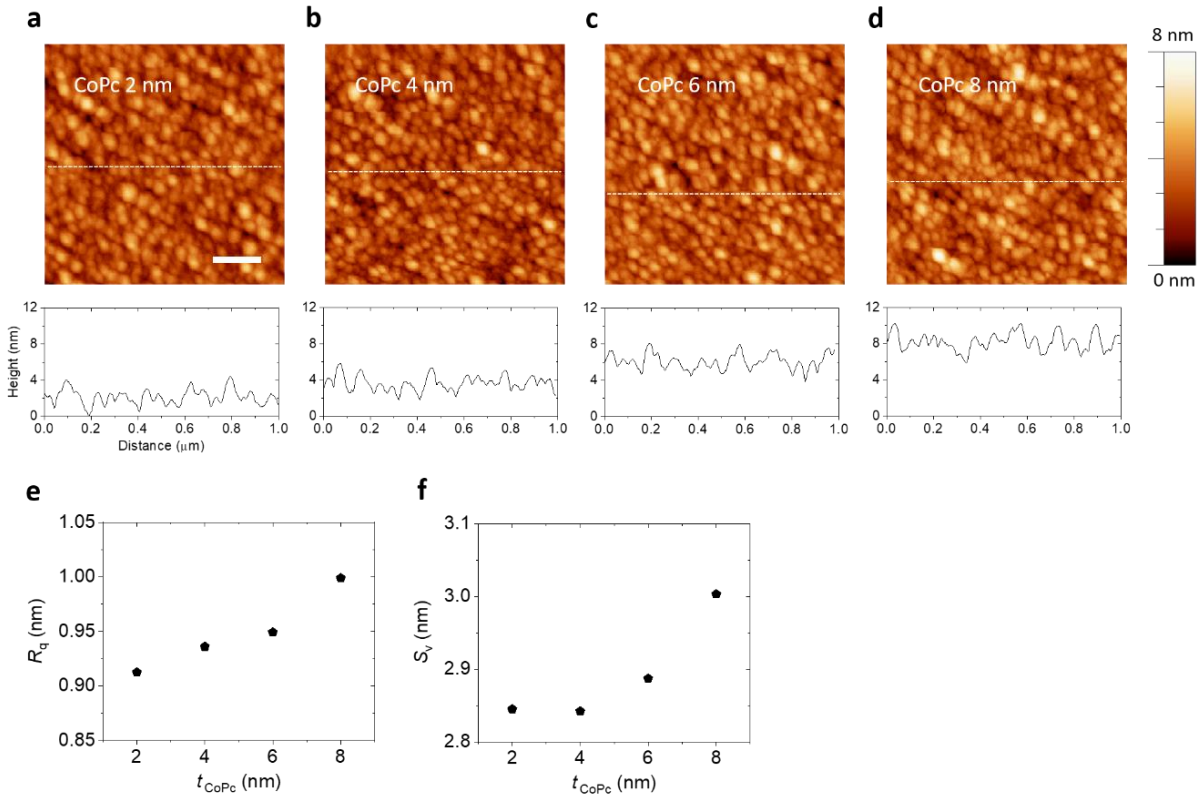

Figure S7. Surface analysis of CoPc layers of different thickness by atomic force microscopy. a-d) Morphology of CoPc films from 2 nm to 8 nm, respectively. The scan size is 1 μm x 1 μm, and the scale bar at the right indicates the *z*-scale for all the images. Below each image, we have plotted the profile of the morphology along a representative white-dot line. We have vertically translated the profile so that the average *z*-value represents the thickness of the CoPc film (2, 4, 6, and 8 nm). e) The root mean square roughness (R_q) of the CoPc layers from 2 nm to 8 nm. The roughness extracted for the different thicknesses is similar, as it gradually increases from 0.9 nm (for CoPc 2 nm) to 1.0 nm (for CoPc 8 nm). f) The maximum pit-height (S_v) of the CoPc layers from 2 nm to 8 nm. In all cases, S_V is higher than 2.8 nm, indicating the 2- and 4-nm-thick layers are not continuous to form antiferromagnetic CoPc layer-by-layer stacks.

Structure (unit : nm)	H_{EB}/H_C	T (K)	AFM type	Reference
FGT(30)/$CrCl_3$(15)	0.2	10	uncompensated	[15]
FGT(30)/$CrCl_3$(45)	0.1	10		
FGT(17)/O-FGT(3)	0.15	70	-	[46]
FGT(38)/O-FGT(3)	0.28	70		
FGT(20)/CoPc(6)	0.34	10	uncompensated	This work
FGT(25)/IrMn(2)	0.04	2	compensated	[47]
FGT(23)/$MnPSe_3$(23)	0.04	10	compensated	[16]
FGT(23)/$MnPS_3$(23)	0.05	10	compensated	
FGT(9)/$MnPS_3$(19)	0.05	10	compensated	[13]

Table S1. H_{EB}/H_C ratio in FGT based exchange bias systems. The ratio is calculated with recorded data in the reference papers. We note that most H_{EB}/H_C reported here are measured at a temperature < 10 K, and are therefore comparable. In the case of the oxidized FGT flake, the low temperature data are not available, so we report the data at 70 K. In our case, at that temperature H_{EB}/H_C is much lower (0.02), as 70 K is not far from the estimated blocking temperature of our CoPc film. We point out that the interface between FGT and oxidized FGT is ill-defined, and it cannot be described as a van der Waals interface.

This table also explains why our molecular system introduces a stronger exchange bias as compared to other van der Waals antiferromagnets. The compounds in the MPX_3 family (used in ref. 13 and 16) are compensated antiferromagnets characterized by an antiferromagnetic coupling of the spins in each layer; therefore they do not couple efficiently to the FGT magnetization. In the same way, the $CrCl_3$ is uncompensated, but the spins are mostly aligned in-plane, whereas the FGT has a strong out-of-plane anisotropy. In our case, CoPc molecules are ideal since (i) when in contact to a ferromagnetic surface, they are prone to couple ferromagnetically to it, and (ii) they are known to form uncompensated antiferromagnetic ordering in thin films.